

Experimental Verification and Graphical Characterization of Dynamic Jamming in Frictional Rigid-Body Mechanics

Daniel Meltz and Yizhar Or and Elon Rimon

Technion, Israel Institute of Technology
smdaniel,izi,rimon@tx.technion.ac.il

Abstract *The dynamics of a rigid body sliding on a frictional contact can have multiple solutions as well as sudden contact-mode transitions. This paper is concerned with dynamic jamming, an event where a sliding rigid body suddenly jams and experiences an impact-like transition into free flying mode. Using a simple experiment that mimics a sliding rigid-body situation, dynamic jamming is recorded for the first time. The phenomenon occurs almost at the theoretical position-and-velocity prediction, indicating that this type of jamming is not a mere artifact of the rigid-body modeling paradigm. A new interpretation of dynamic jamming is offered in terms of the body's instantaneous acceleration center. Once this center reaches a graphically determinable jamming line, the body ceases its sliding mode and experiences a dynamic jamming event. Based on this insight, some ways to prevent dynamic jamming are discussed.*

1 Introduction

This paper considers a rigid body sliding against a frictional contact. If the sliding body possesses certain inertial parameters and contact friction is sufficiently high, the body's dynamic solution can reach a jamming event. During this event the sliding contact suddenly sticks, and the body experiences an impact-like transition into free flying mode. This paper provides experimental evidence that such jamming events occur in the physical world. Jamming is of great concern to manipulation and assembly planners, as well as to multi-legged locomotion planners. In legged locomotion, small foot placement errors can result in contacts sliding to a nearby stable posture. An event where a sliding foot suddenly jams and breaks contact can be catastrophic for a legged robot. This paper strives to better understand the phenomenon in order to ensure reliable and safe planners.

The classical Coulomb friction model is an excellent approximation for the physical world. However, it specifies the contact reaction force in terms of inequalities in the body's configuration and velocity, leading to the possibility of non-unique so-

lutions and abrupt contact-mode transitions. Such possibilities were first noted by Painlevé (1895, [7]), who noted that the dynamic solution for a slender rigid rod sliding against a flat support can become ill-defined. This phenomenon has been formally studied by [3, 5, 10]. In robotics, the phenomenon is first discussed by Erdmann [2] and Rajan et al. [9] in the context of assembly planning. The mechanics of contact jamming has been independently characterized by Dupont [1], who suggested the term *dynamic jamming* for this phenomenon. Wang and Mason [6, 12] demonstrated that when a sliding solution ceases to exist, the body's subsequent behavior can be explained as a *tangential impact* which results in contact breakage. Other relevant papers discuss contact-mode transitions in the context of multi rigid body simulation e.g., [4, 8]. However, there has been a debate whether dynamic jamming is a truly physical phenomenon, or perhaps only a shortcoming of the ideal rigid-body modeling paradigm.

This paper makes two contributions. First, it provides an experimental evidence that dynamic jamming is a physical phenomenon. The experiment involves a kinematic chain sliding on an inclined plane, with the chain's parameters mimicking a sliding rigid-body situation. Second, the paper offers a geometric characterization of dynamic jamming in terms of the body's instantaneous acceleration center, first discussed by Wang and Mason [6]. The body's instantaneous acceleration center traces a curve during its sliding motion. Once this curve reaches a graphically determinable *jamming line*, a dynamic jamming event takes place.

The structure of the paper is as follows. The next section reviews the dynamic jamming condition for a single sliding contact. Section 3 describes the experimental system and derives its dynamic jamming condition. Section 4 describes results of the experiments. Section 5 provides a geometric interpretation of dynamic jamming in terms of the body's instantaneous acceleration center. The concluding section discusses ways to prevent jamming in applications.

2 Dynamic Jamming Condition

This section summarizes the dynamic jamming condition. Consider a kinematic chain \mathcal{K} made of several rigid bodies. We assume that one body of \mathcal{K} maintains a sliding contact with a fixed surface of the environment, denoted \mathcal{A} . We assume Coulomb friction at the contact, and assume that gravity or some other force maintains the sliding motion during a time interval.

Dynamic jamming results from interaction of the chain's dynamics with the kinematic constraint imposed by the sliding contact. The chain's dynamics takes place in its constrained configuration space, or *c-space*, defined as follows. Let \mathcal{K} have n degrees of freedom and let $q \in \mathbb{R}^n$ denote its configuration. Let $\mathcal{K}(q)$ denote the physical points occupied by \mathcal{K} when it is at a configuration q . The fixed surface \mathcal{A} induces a c-space obstacle, or *c-obstacle*, defined as $\mathcal{CA} = \{q \in \mathbb{R}^n : \mathcal{K}(q) \cap \mathcal{A} \neq \emptyset\}$. Let $\text{bdy}(\mathcal{CA})$ denote the boundary of \mathcal{CA} . The chain's c-space is the union of its free-flying configurations, $\mathbb{R}^n - \mathcal{CA}$, with its sliding configurations, $\text{bdy}(\mathcal{CA})$. In the following, $\boldsymbol{\eta}(q)$ denotes the outward unit normal to $\text{bdy}(\mathcal{CA})$ at q .

In order to write the chain's dynamics, we need notation for the generalized force induced on the chain by the contact force. Let x denote the contact point, and let f_n and f_t denote the normal and tangent reaction forces at x . Let $\lambda = \|f_n\|$ denote the normal force magnitude. During sliding the net reaction force lies on the friction-cone edge opposing the direction of sliding. Hence $\|f_t\| = \mu\|f_n\|$ where μ is the coefficient of friction. The generalized force induced by f_n is a positive multiple of $\boldsymbol{\eta}(q)$, and is given by

$$\mathbf{f}_n(q) = \lambda \hat{\mathbf{f}}_n(q) \quad q \in \text{bdy}(\mathcal{CA}),$$

where $\hat{\mathbf{f}}_n(q)$ is the generalized force induced by a unit-magnitude normal force. Note that $\lambda \geq 0$ is a free parameter at this stage. The generalized force induced by f_t has no obvious c-space interpretation, and is given by

$$\mathbf{f}_t(q) = \mu s \lambda \hat{\mathbf{f}}_t(q) \quad q \in \text{bdy}(\mathcal{CA}),$$

where $\hat{\mathbf{f}}_t(q)$ is the generalized force induced by a unit-magnitude tangential force, and $s = \pm 1$ is a sign variable set to oppose the direction of sliding. Let $\mathbf{f}_g(q) \in \mathbb{R}^n$ and $\boldsymbol{\tau}(t) \in \mathbb{R}^n$ denote the generalized forces induced by gravity and joint torque controls. Then the dynamics of \mathcal{K} is given by

$$M(q)\ddot{q} + h(q, \dot{q}) = \lambda(\hat{\mathbf{f}}_n(q) + \mu s \hat{\mathbf{f}}_t(q)) + \mathbf{f}_g(q) + \boldsymbol{\tau}(t),$$

where $M(q)$ is the chain's $n \times n$ inertia matrix, and $h(q, \dot{q}) \in \mathbb{R}^n$ are Coriolis and centripetal forces.

Next consider the constraint imposed by the sliding contact. Since \mathcal{K} maintains continuous contact

with the surface of \mathcal{A} , its trajectory $q(t)$ lies on $\text{bdy}(\mathcal{CA})$ during sliding. It follows that $\dot{q}(t)$ is tangent to the boundary of \mathcal{CA} . Hence $\boldsymbol{\eta}(q(t)) \cdot \dot{q}(t) = 0$ during sliding. Taking the derivative of both sides gives the sliding constraint $\boldsymbol{\eta}(q) \cdot \ddot{q} + \dot{q}^T D\boldsymbol{\eta}(q)\dot{q} = 0$. Substituting for \ddot{q} according to the chain's dynamics gives a linear equation in λ ,

$$\begin{aligned} \boldsymbol{\eta}(q)^T M(q)^{-1} (\hat{\mathbf{f}}_n(q) + \mu s \hat{\mathbf{f}}_t(q)) \lambda = \\ \boldsymbol{\eta}(q)^T M(q)^{-1} (\mathbf{f}_g(q) + \boldsymbol{\tau}(t) - h(q, \dot{q})) - \dot{q}^T D\boldsymbol{\eta}(q)\dot{q}. \end{aligned}$$

The equation specifies a finite solution for $\lambda = \|\mathbf{f}_n\|$ as long as the coefficient multiplying λ is non-vanishing. The vanishing of this coefficient is the dynamic jamming condition.

Lemma 2.1 ([1]). *Let a chain \mathcal{K} slide against a fixed surface \mathcal{A} with Coulomb friction at the contact. The chain experiences **dynamic jamming** when its trajectory $q(t)$ reaches the constraint*

$$\boldsymbol{\eta}(q)^T M(q)^{-1} (\hat{\mathbf{f}}_n(q) + \mu s \hat{\mathbf{f}}_t(q)) = 0, \quad (1)$$

where $\boldsymbol{\eta}(q)$ is the c-obstacle normal and $\hat{\mathbf{f}}_n(q) + \mu s \hat{\mathbf{f}}_t(q)$ is the generalized force induced by the contact force.

Note that $s = \pm 1$, depending on the sliding direction. For a fixed value of s , condition (1) depends solely on the chain's configuration q . When $q(t)$ reaches this constraint, $\|\mathbf{f}_n\|$ becomes unbounded and the chain experiences a *tangential impact* [12]. The impact consists of an initial sliding phase during which the contact switches to rolling (also called tangential sticking). The impact proceeds through compression and restitution phases, terminating in contact breakage and transition of the chain into free flying mode.

3 Experimental Jamming System

This section describes the experimental system and characterizes its dynamic jamming condition. This condition gives the set of initial positions-and-velocities that carries the chain into dynamic jamming, which is the basis for the experiments described in the next section.

3.1 System Description

The experimental system, sketched in Figure 1, consists of a kinematic chain sliding on an inclined plane under the influence of gravity. The chain consists of a rectangular plate which maintains the sliding contact, hinged to a cylindrical body which resembles Painleve's rod. The plate's thickness is $e = 10$ mm and its length is 290 mm. It is made of light material (epoxy enforced balsa), which weighs $m_1 = 0.23$ kg and has radius of gyration $\rho_1 = 83.8$ mm. The hinge

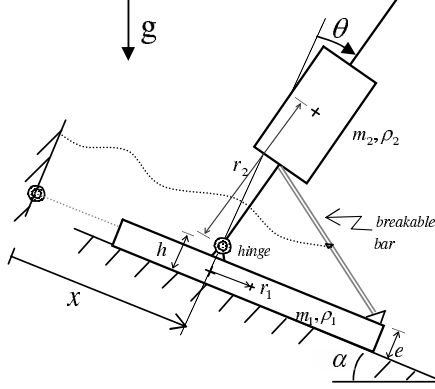


Figure 1: Schematic view of experimental system.

is mounted at a distance of 90 mm from the plate's rear-end, at a height of $h = 17$ mm above the inclined plane (see figure). The cylindrical body is made of steel, and two cylinders were prepared for the experiment. The two cylinders weigh $m_2 = 1.07$ and $m_2 = 4.65$ kg with radius of gyration $\rho_2 = 51.2$ and $\rho_2 = 38.5$ mm. The center of mass of both cylinders is at a distance $r_2 = 209$ mm from the hinge. The inclined plane has a slope $\alpha = 30^\circ$, and the dynamic coefficient of friction is $\mu = 0.64 \pm 5\%$.

As discussed below, the chain's jamming is determined by two configuration variables—the sliding plate's distance x , and the hinge's angle θ . Each of these variable is measured with its own optical encoder. Once the chain attains a sufficiently large initial sliding velocity, a specific initial θ interval leads the chain into dynamic jamming. In order to enforce these initial conditions, the hinge is initially locked with a nearly massless rigid bar (weighing less than 10 gr) at a desired initial angle. The bar is attached with a wire to the environment. When the wire becomes fully stretched, the locked chain achieves the required initial sliding velocity and the wire breaks the locking bar. From this stage onward $x(t)$ and $\theta(t)$ are recorded until dynamic jamming is achieved.

3.2 System Jamming Condition

We now compute the chain's dynamic jamming condition. The experiment is designed such that motion takes place in a planar environment. The chain's configuration is described using the following three frames. A fixed world frame attached to the inclined slope, with its positive x direction pointing downward. A plate frame attached at its middle line just below the hinge, and a cylindrical-body frame attached at the hinge point. Using these frames, the chain's configuration is $q = (x, y, \psi, \theta)$, where (x, y, ψ) are the plate's position and orientation and θ is the hinge's angle. The angle θ is measured in clock-

wise direction with respect to the inclined-plane's normal (Figure 1). In the following, $r_1 = 55$ mm is the distance from the plate's origin to its center of mass, and $l = h - e/2 = 12$ mm is the hinge's height above the plate's origin. The chain's inertia matrix is given by

$$M(q) = \begin{bmatrix} m_1 + m_2 & 0 & m_2 l & m_2 r_2 c\theta \\ 0 & m_1 + m_2 & -m_1 r_1 & -m_2 r_2 s\theta \\ m_2 l & -m_1 r_1 & m_1(r_1^2 + \rho_1^2) + m_2 l^2 & m_2 l r_2 c\theta \\ m_2 r_2 c\theta & -m_2 r_2 s\theta & m_2 l r_2 c\theta & m_2(r_2^2 + \rho_2^2) \end{bmatrix}$$

where $s\theta = \sin\theta$ and $c\theta = \cos\theta$. Based on a ZMP argument [11], the net normal reaction force acting on the base-plate is equivalent to a single force acting at a distance ξ from the plate's origin. The generalized force induced on the chain by a unit normal force acting at a distance ξ is $\mathbf{f}_n(q) = (0, 1, \xi, 0)$. The sliding direction in the experiment is always along the positive x coordinate. Hence the generalized force induced by a unit tangential force opposing the sliding direction is $\mathbf{f}_t(q) = -(1, 0, e/2, 0)$. Since the contact normal $\boldsymbol{\eta}(q)$ is a positive multiple of $\mathbf{f}_n(q)$, the dynamic jamming condition of Lemma 2.1 is: $\mathbf{f}_n(q)^T M(q)^{-1} ((\mathbf{f}_n(q) - \mu \mathbf{f}_t(q))) = 0$. Substituting for $M(q)$, $\mathbf{f}_n(q)$, $\mathbf{f}_t(q)$ gives the chain's dynamic jamming condition:

$$\left(1 + \frac{m_1}{m_2}\right) \left(1 + \frac{\rho_2^2}{r_2^2}\right) - \cos^2\theta + \mu \sin\theta \cos\theta = 0, \quad (2)$$

where θ varies in the interval $[-\pi/2, \pi/2]$. If one substitutes $m_1 = 0$ in (2), one obtains Dupont's single-body dynamic jamming condition [1]. Since $m_1 \ll m_2$ in the experiment, the chain provides a reasonable approximation for a single-body dynamic jamming experiment. In order to solve (2) for θ , let $\theta_f = \tan^{-1}(\mu)$. Then (2) becomes

$$2\left(1 + \frac{m_1}{m_2}\right) \left(1 + \frac{\rho_2^2}{r_2^2}\right) - 1 = \sqrt{1 + \mu^2} \cos(2\theta + \theta_f). \quad (3)$$

The equation has either zero or two solutions in $[-\pi/2, \pi/2]$. It has two solutions iff $2\left(1 + \frac{m_1}{m_2}\right)\left(1 + \frac{\rho_2^2}{r_2^2}\right) - 1 \leq \sqrt{1 + \mu^2}$. The latter inequality implies that the sliding chain possesses dynamic jamming angles if the contact friction is sufficiently high. In the experiments, we verify dynamic jamming for $m_1 = 0.23$ kg, $m_2 = 4.65$ kg, $\rho_2 = 38.5$ mm, $r_2 = 209$ mm, and $\mu = 0.64$. The jamming angles for these values are $\theta_{J1} = -21.16^\circ$ and $\theta_{J2} = -11.45^\circ$.

For these parameter values, we first determined the initial θ values, denoted $\theta(0)$, that lead the chain to θ_{J1} or θ_{J2} . The results are summarized in Figure 2. The figure shows the contact normal, the friction cone edges, and two lines aligned with θ_{J1} and

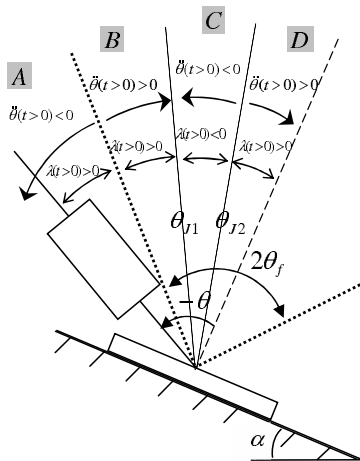


Figure 2: Mapping of initial hinge angles that lead the chain to the jamming angles.

θ_{J2} . These lines induce a partition of $\theta(0)$ into four qualitatively distinct regions. In all of these regions $\dot{\theta}(0) = 0$, while $\dot{x}(0)$ is sufficiently large as detailed below. Trajectories starting in region A rotate the hinge away from θ_{J1} . Region B is the desired one. Trajectories starting in this region rotate the hinge towards θ_{J1} while continuously maintaining a sliding contact. Initial angles in region C rotate the hinge toward θ_{J1} , but a sliding contact is not maintained during these motions. Initial angles in region D rotate the hinge away from θ_{J2} . The jamming region thus corresponds to region B, which consists of the interval $-32.62^\circ \leq \theta(0) \leq -21.16^\circ$. Finally, the initial sliding velocity needs to be sufficiently high as to maintain the chain's downward sliding up to the jamming event. Dynamic simulations with $\theta(0)$ varying in region B determined the required initial sliding velocity to be $\dot{x}(0) \geq 1.5$ m/sec.

4 Experimental Results

This section describes two experiments. A control experiment that involves no jamming, and a dynamic jamming experiment. The experiments differ only by the properties of the cylindrical body. Both experiments share the values $m_1 = 0.23$ kg, $r_2 = 209$ mm, and $\mu = 0.64$. The control experiment was executed with the light-weight cylindrical body of mass $m_2 = 1.07$ kg and radius of gyration $\rho_2 = 51.2$ mm. Substituting these values in (3) gives no jamming angles. The jamming experiment was executed with the heavy-weight cylindrical body of mass $m_2 = 4.65$ kg and radius of gyration $\rho_2 = 38.5$ mm. These values are expected to give jamming at $\theta_{J1} = -21.16^\circ$.

The results of the experiments are shown in Figure 3. The upper graphs show the evolution of

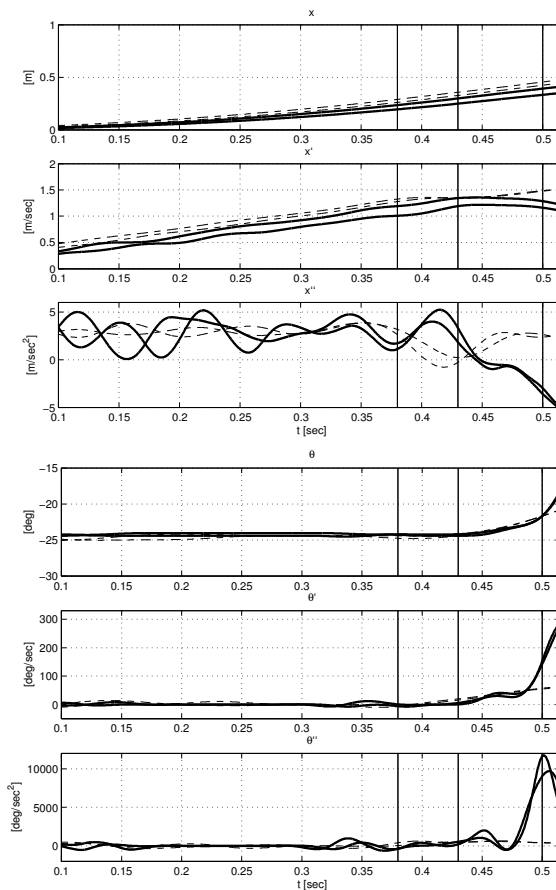


Figure 3: Measurements of x, \dot{x}, \ddot{x} and $\theta, \dot{\theta}, \ddot{\theta}$ for non-jamming (dashed lines) and jamming (solid lines).

x, \dot{x}, \ddot{x} ; the lower graphs show the evolution of $\theta, \dot{\theta}, \ddot{\theta}$. The results of two control experiments are depicted with dashed lines. These experiments started at $t = -0.05$ sec with the hinge at $\theta = -24.4^\circ$. The locking bar was broken at $t = 0.28$ sec. The graphs indicate that the chain continued its sliding without any singular event in x and θ . The results of two jamming experiments are depicted with solid lines. These experiments started at $t = -0.02$ sec with the hinge at $\theta = -24.4^\circ$. The locking bar was broken at $t = 0.33$ sec. The graphs indicate a singular event during the interval $0.48 \leq t \leq 0.50$ sec. The event involves a steep decrease of \ddot{x} to a negative acceleration of -4 m/sec², accompanied by a steep increase of $\ddot{\theta}$ to a clockwise acceleration of $10,000 - 12,000$ deg/sec². The value of θ during this interval is $-22.5^\circ \leq \theta \leq -21.0^\circ$. This interval contains the theoretical jamming angle at $\theta_{J1} = -21.16^\circ$.

Several snapshots of the experiments appear in Figure 4. The figure shows side-by-side three frames taken from each experiment. The first frame shows the chain sliding as a single rigid body in order to



Figure 4: Successive frames of (a) non-jamming, and (b) jamming experiments.

gain the required initial sliding velocity. The second frame shows the instant where the locking bar breaks and releases the chain’s hinge. The third frame was taken a couple of milliseconds after $t = 0.48$ sec. While the control experiment shows the chain continuing its sliding mode, the picture of the jamming experiment is strikingly different. First, the chain’s base plate rolls about its forward tip, as predicted by a tangential impact scenario [12]. Second, the chain lifts into a free flying mode, with a small gap opening between the base plate and the supporting plane. This behavior is again consistent with a tangential impact scenario, which predicts contact breakage whenever the coefficient of restitution is non-plastic.

5 Geometric Characterization of Dynamic Jamming

This section provides a geometric characterization of dynamic jamming for a planar body, denoted \mathcal{B} , sliding against a fixed linear segment, denoted \mathcal{A} . Let \mathcal{B} move along a c-space trajectory $q(t) = (d(t), \theta(t))$. Let r denote a point of \mathcal{B} described in its body frame, and let x denote the same point described in a fixed world frame. When \mathcal{B} is at a configuration q , the relation of x to r is: $x = X(r, q) = R(\theta)r + d$, where $R(\theta)$

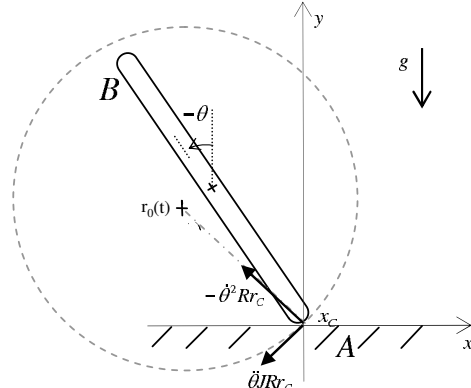


Figure 5: Instantaneous center of acceleration $r_0(t)$.

is \mathcal{B} ’s orientation matrix. In the following, $X_r(q)$ denotes the transformation X such that r is held fixed.

A moving rigid body possesses an *instantaneous acceleration center*, which is denoted r_0 and depends on q, \dot{q}, \ddot{q} . When \mathcal{B} ’s frame origin is selected at r_0 , the acceleration of any point $r \in \mathcal{B}$ is given by $\ddot{X}_r(q) = \ddot{\theta} J R r - \dot{\theta}^2 R r$, where $J = \begin{bmatrix} 0 & -1 \\ 1 & 0 \end{bmatrix}$ (see Figure 5). Let r_c denote the current contact point, expressed in \mathcal{B} ’s body frame, and let $x_c = X_{r_c}(q)$. The following lemma characterizes dynamic jamming in terms of \mathcal{B} ’s instantaneous acceleration center.

Lemma 5.1. *Let a planar body \mathcal{B} slide against a linear segment \mathcal{A} , and let x_c be the current contact point. Then **dynamic jamming** takes place when \mathcal{B} ’s instantaneous center of acceleration reaches with a non-vanishing $\dot{\theta}$ the normal line passing through x_c .*

Proof: Let \mathcal{B} ’s body frame be at the current acceleration center r_0 , and let $x_0 = X_{r_0}(q)$. Since \mathcal{B} ’s origin is at r_0 , $\ddot{X}_{r_c}(q) = \ddot{\theta} J R r_c - \dot{\theta}^2 R r_c$. Substituting $R r_c = x_c - x_0$ gives $\ddot{X}_{r_c}(q) = [\ddot{\theta} J - \dot{\theta}^2 I](x_c - x_0)$, where I is the 2×2 identity matrix. Since x_c slides along a flat segment, \dot{X}_{r_c} and \ddot{X}_{r_c} are aligned with the segment’s unit tangent, denoted \hat{t} . Thus $\ddot{X}_{r_c}(q) = \pm \|\ddot{X}_{r_c}\| \hat{t}$. Equating the two expressions for $\ddot{X}_{r_c}(q)$ gives

$$\pm \|\ddot{X}_{r_c}\| \hat{t} = [\ddot{\theta} J - \dot{\theta}^2 I](x_c - x_0). \quad (4)$$

Let \hat{n} be a unit vector normal to \mathcal{A} . Multiplying both sides of (4) with \hat{n} gives: $\ddot{\theta} \hat{t} \cdot (x_c - x_0) - \dot{\theta}^2 \hat{n} \cdot (x_c - x_0) = 0$, where we used the identity $J \hat{n} = -\hat{t}$. Solving this equation for $\ddot{\theta}$ gives

$$\ddot{\theta} = \frac{\hat{n} \cdot (x_c - x_0)}{\hat{t} \cdot (x_c - x_0)} \dot{\theta}^2. \quad (5)$$

The reaction force during sliding is $\|f_n\|(\hat{n} + s\mu\hat{t})$, where $s = \pm 1$. The magnitude $\|f_n\|$ is determined by the row governing θ in \mathcal{B} ’s sliding dynamics,

$$m\rho^2\ddot{\theta} = \|f_n\|(x_c - x_0)^T J(\hat{n} + s\mu\hat{t}) + \tau_{ext}, \quad (6)$$

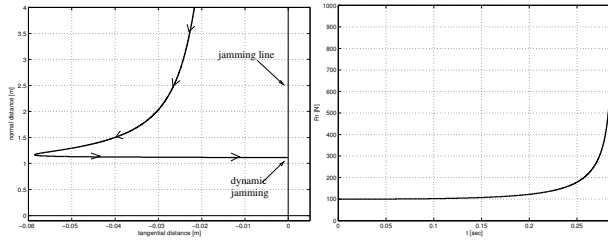


Figure 6: (a) \mathcal{B} 's center of acceleration, and (b) normal force magnitude during sliding.

where m and ρ are \mathcal{B} 's mass and radius of gyration. Substituting the expression for $\ddot{\theta}$ from (5) into (6),

$$\|f_n\|(x_c - x_0)^T J(\hat{n} + s\mu\hat{t}) = m\rho^2 \frac{\hat{n} \cdot (x_c - x_0)}{\hat{t} \cdot (x_c - x_0)} \dot{\theta}^2 - \tau_{ext}.$$

The term multiplying $\|f_n\|$ is always finite. Since τ_{ext} is also finite and $\dot{\theta}$ is assumed to be non-vanishing, the condition $\hat{t} \cdot (x_c - x_0) = 0$ implies that $\|f_n\| = \infty$. The latter condition determines the jamming line. \square

Example. Consider the sliding rod depicted in Figure 5. The rod has length $l = 2$ m, mass $m = 10$ kg, and radius of gyration $\rho = 0.2$ m. The coefficient of friction is $\mu = 0.5$. The rod's initial conditions are $x(0) = 0.55$ m, $y(0) = 0.89$ m, $\theta(0) = -26.5^\circ$, $\dot{x}(0) = -100$ m/sec, and $\dot{y}(0) = \dot{\theta}(0) = 0$. Figure 6(a) plots the rod's acceleration center, $x_0 = X_{r_0}(q)$, during sliding motion under gravity. The initial conditions are selected such that $x_0(0)$ lies on the jamming line. Since $\dot{\theta}(0) = 0$, no dynamic jamming takes place at $t = 0$. The rod subsequently slides to the right, while x_0 moves leftward. As the sliding motion proceeds, x_0 reaches the jamming line at which point dynamic jamming takes place. A plot of $\|f_n\|$ up to the jamming event appears in Figure 6(b).

6 Conclusion

The paper described an experiment of a chain sliding under the influence of gravity against a frictional contact. The chain's parameters mimic a sliding rod situation, and for these parameter values the theory predicts dynamic jamming at a hinge angle $\theta = -21.16^\circ$. The actual experiment showed a singular event taking place in the interval $-22.5^\circ \leq \theta \leq -21.0^\circ$. The singular event started with a transition of the chain from sliding to tangential sticking, followed by transition into a free flying mode. This scenario is consistent with a tangential impact scenario [6]. The matching between theory and experiment indicates that dynamic jamming is not an artifact of the rigid-body modeling paradigm, but a truly physical phenomenon. The paper also characterized dynamic jamming of a sliding planar body as an event where the

body's instantaneous acceleration center reaches the normal line passing through the current contact.

The dynamic jamming condition (3) provides the following insight. First, any chain or rigid body can experience dynamic jamming if friction at the contact is sufficiently high. Second, for any fixed value of the coefficient of friction, one can purposely design the chain or body such that it would *not* experience dynamic jamming. In the single-body case, the ratio ρ/r must be sufficiently large in order to avoid jamming. In the chain case, one can additionally prevent dynamic jamming by ensuring that m_1/m_2 is sufficiently large. This requires that the chain's base-plate mass would dominate its upper-body mass.

References

- [1] P. E. Dupont and S. P. Yamajako. Jamming and wedging in constrained rigid-body dynamics. In *ICRA*, 2349–2354, 1994.
- [2] M. A. Erdmann. On a representation of friction in configuration space. *Int. J. of Robotics Research*, 13(3):240–271, 1994.
- [3] F. Génot and B. Brogliato. New results on painlevé paradoxes. *European J. of Mechanics—A/Solids*, 18(4):653–677, 1999.
- [4] P. R. Kraus, V. Kumar, and P. Dupont. Analysis of frictional contact models for dynamic simulation. In *ICRA*, 2822–2827, 1998.
- [5] P. Lotstedt. Coulomb friction in two-dimensional rigid body systems. *Zeitschrift für Angewandte Mathematik und Mechanik*, 61:605–615, 1981.
- [6] M. T. Mason and Y. Wang. On the inconsistency of rigid-body frictional planar mechanics. In *ICRA*, 524–528, 1988.
- [7] P. Painlevé. Sur les lois du frottement de glissement. *Comptes Rendus De L'Académie Des Sciences*, (121):112–115, 1895.
- [8] J. S. Pang and J. C. Trinkle. On dynamic multi-rigid-body contact problems with coulomb friction. *Zeitschrift für Angewandte Mathematik und Mechanik*, 77(4):267–279, 1997.
- [9] V. T. Rajan, R. Burrige, and J. T. Schwartz. Dynamics of rigid body in frictional contact with rigid walls. In *ICRA*, 671–677, 1987.
- [10] D. E. Stewart. Convergence of a time-stepping scheme for rigid-body dynamics and resolution of Painlevé's problem. *Arch. Rational Mechanics Anal.*, 14(3):466–475, 1998.
- [11] M. Vukobratovic and B. Borovac. Zero moment point — thirty five years of its life. *Int. J. of Humanoid Robotics*, 1(1):157–173, 2004.
- [12] Y. Wang and M. T. Mason. Two-dimensional rigid body collisions with friction. *J. of Applied Mechanics*, 59:635–642, 1992.